Thesis for the Degree of Master of Engineering

A preclinical study on airway remodeling under methacholine provocation using OCT and CT with breath-hold techniques

by

Yikeun Kim

Department of Biomedical Engineering

The Graduate School

Pukyong National University

August 2016

A preclinical study on airway remodeling under methacholine provocation using OCT and CT with breath-hold techniques

(메타콜린 유발 기도 개형 토끼모델에서 호흡정지 기법이 적용된 OCT와 CT 를 이용한 천식 연구)

Advisor: Prof. Yeh-Chan Ahn

By

Yikeun Kim

A thesis submitted in partial fulfillment of the requirements
for the degree of

Master of Engineering

in Department of Biomedical Engineering,
The Graduated School,
Pukyong National University

August 2016

Thesis for the Degree of Master of Engineering

A dissertation

by

Yikuen Kim

Approved by:

_____

(Chairman) Sung Won Kim

_____ _____

(Member) Chulho Oak (Member) Yeh-Chan Ahn

August 22, 2016

Table of Contents

List of Figures

List of Table

메타콜린 유발 기도 개형 토끼모델에서 호흡정지 기법이 적용된
OCT 와 CT 를 이용한 천식 연구

김이근

부경대학교 대학원 바이오메디컬공학과

요약

많은 천식 연구들이 CT 이미지 분석을 통해서 실시되어왔다. 그러나 천식의 발병원인은 아직도 명확하게 밝혀지지 않았다. 이 논문의 목적은 인공호흡기로 실시된 들숨과 날숨 상태에서 실험체의 호흡을 정지시킨 폐의 이미지에 관한 새로운 방법의 연구이다.

이 논문에 사용된 이미징 기술은 CT와 OCT이다. CT는 X-ray 이미지를 여러층으로 분석한다. 그리고 OCT는 인체에 무해하고 높은 해상도를 가지고 있는 이미지 신기술이다. 연구에서는 폐와 폐포를 호흡정지 상태에서 조사하기 위해 CT와 OCT를 사용하였다. 인공호흡기로 실시된 호흡정지 기법은 동물실험에서 호흡으로 인한 잡음을 제거한 영상을 수집 및 분석 할 수 있었다.

피실험는 메카콜린으로 실험체 토끼의 기도 개형이 유도되었다. 마취 후 최대압력이 17cmH2O인 정상호흡으로 실시되었다. 호기는 최대압력 28cmH2O에서 시행되었다. 호흡정지는 호흡수를 15에서 0으로 조작하면서 실시되었다. 같은 방식으로 호기시 호흡정지는 최대압력 7cmH2O에서 실시되었다. 두 호흡정지 상태에서 CT와 OCT이미지는 폐와 폐포에서 중요한 결과가 관찰되었다.

I. Introduction

1 Motivation from asthma

Typical non-communicable disease, asthma is a chronic respiratory problem that causes wheezing, chest tightness, and shortness of breath. (Steen et al. 1994; Moffatt et al. 2010) Globally 235 million people suffer from asthma currently. (WHO, November 2013) It occurs in both developed and developing countries, but most of the deaths are related to low- and lower-middle income countries. However, allergic diseases such as asthma have increased in the westernized countries than underdeveloped countries in recent decades.(Beasley et al. 1998) The prevalence is more common to westernized societies. Poor of developed countries and rich of developing countries have high prevalence rate.(Wills-Karp, Santeliz, and Karp 2001) This is closely related to lifestyle, such as the accessibility of the medical or exposure to antigen asthma. (Akbari, DeKruyff, and Umetsu 2001) This phenomenon is speculated due to change environment by a result of modernization. (Etzel 2003) It can be expected to continually increase to allergic diseases and asthma forward. The prevalence has increased to childhood asthma and allergic diseases in westernized Korea.(Ahn et al. 2011) Figure I .1 shows the annual fatality rate and prevalence of asthma. Figure I .2 shows asthma world mortality rates.

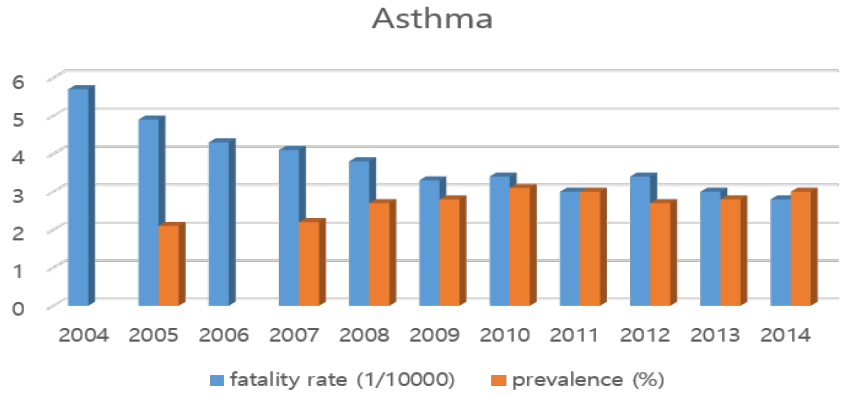

Figure I.1 Annual prevalence and fatality rate of asthma.

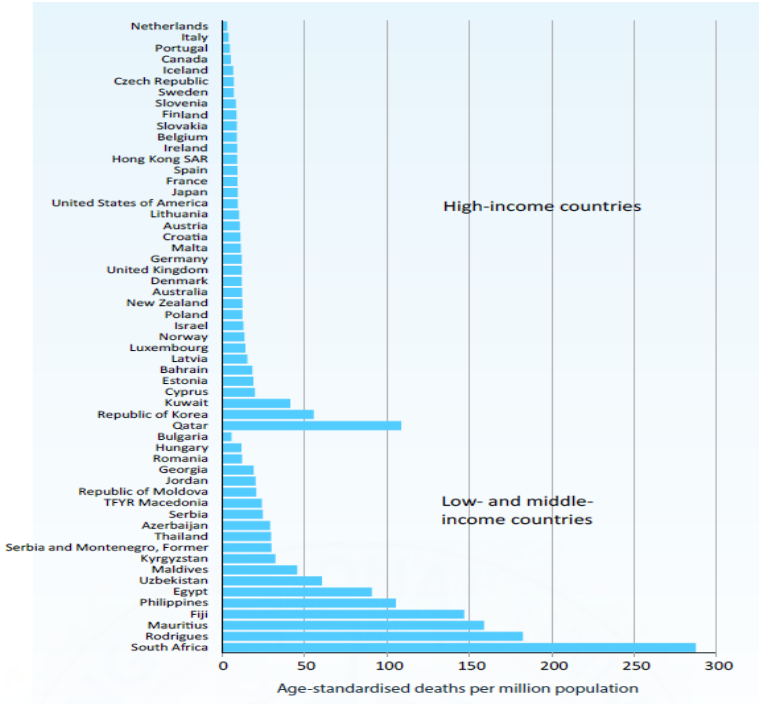

Figure I.2 Asthma mortality rate and country income group for all ages 2001-2010. (Source:The global asthma report 2014)

Genetic studies of asthma have also been actively underway after the Human Genome Project, not along genetic but environmental factors influenced the etiology of asthma.(Zhang, Paré, and Sandford 2008) Acquired genetic effects which were interacted with the environment is regarded more stronger than innate genetic effects.(Miller and Ho 2008) There is a need to study the physical changes or influence due changed environment factors. Many researchers have been studying images related to asthma from CT and MRI.(Gupta et al. 2010; Aysola et al. 2010; Thomas et al. 2009) However etiology and mechanism is uncertainty, thus there is a limit of the therapy and diagnosis.

This study proposes a method using CT and OCT imaging analysis with airway remodeling under methacholine provocation in rabbit model which is different from the heat treatment study that uses OCT to take airway images. (Lam et al. 2013; Coxson et al. 2008) Methacholine has already been used in the diagnosis of asthma that may lead to artificial airway remodeling.

2 Optical coherence tomography (OCT)

Optical coherence tomography (OCT) was developed by the Fujimoto Group of MIT in 1991. (Huang et al. 1991) Initially been produced based on the Michelson interferometer, it could make a 2D image. This is a non-invasive way to view the human body without cutting the human body, or stain process similar to the X-ray. (Schmitt 1999) Early in the OCT it had taken a lot of time to create an image as an initial X-ray film processing to take a long time. The image processing speed was significantly raised after the OCT in the frequency domain was developed. The medical community has an interest in this technology because the technology enables video output in real time. (Chinn, Swanson, and Fujimoto 1997; de Boer et al. 2003; Leitgeb, Hitzenberger, and Fercher 2003; Golubovic et al. 1997) OCT is safety compared to traditional equipment, such as X-ray or MRI. (Fujimoto et al. 1995) OCT has been developing the field of diagnostic techniques. It' s cheap technology compared to the other techniques. (Puliafito et al. 1995; Fercher et al. 2003)

OCT has a limitation that can penetrate the depth direction according to the subject by the properties of visible light. OCT is being developed such as skin, respiratory diseases and endoscopic system using an optical fiber.(G J Tearney et al. 1997; GAMBICHLER et al. 2005; Guillermo J Tearney et al. 1997; Jung et al. 2007; Pitris et al. 1998; Williamson et al. 2011; Welzel et al. 1997)

This study was effectuated to develop airway remodeling under methacholine provocation as mentioned above to targeting the New Zealand rabbit model to determine the potential for the diagnosis of asthma using OCT technology. At the same time experimenter was evaluated the size of alveoli and the overall image of pulmonary in each inspiration and expiration state by applied the method of the ventilator breath-hold.

II. Materials

1 Principle of spectral-domain optical coherence tomography (SDOCT)

SD-OCT used in this study was used 2×2 coupler based Michelson interferometer, that consists of the sample, reference, light source, detector arm focusing on the coupler. The light source generated a low-coherence light and divided into fifty-fifty through coupler. The divided light went to sample and reference arm. The light was reflected by a perfect reflective mirror in Reference arm. And B-mode scan generated the same distance in sample arm by a 2-axis galvanometer. Figure Ⅱ.1 shows The schematic diagram of OCT.

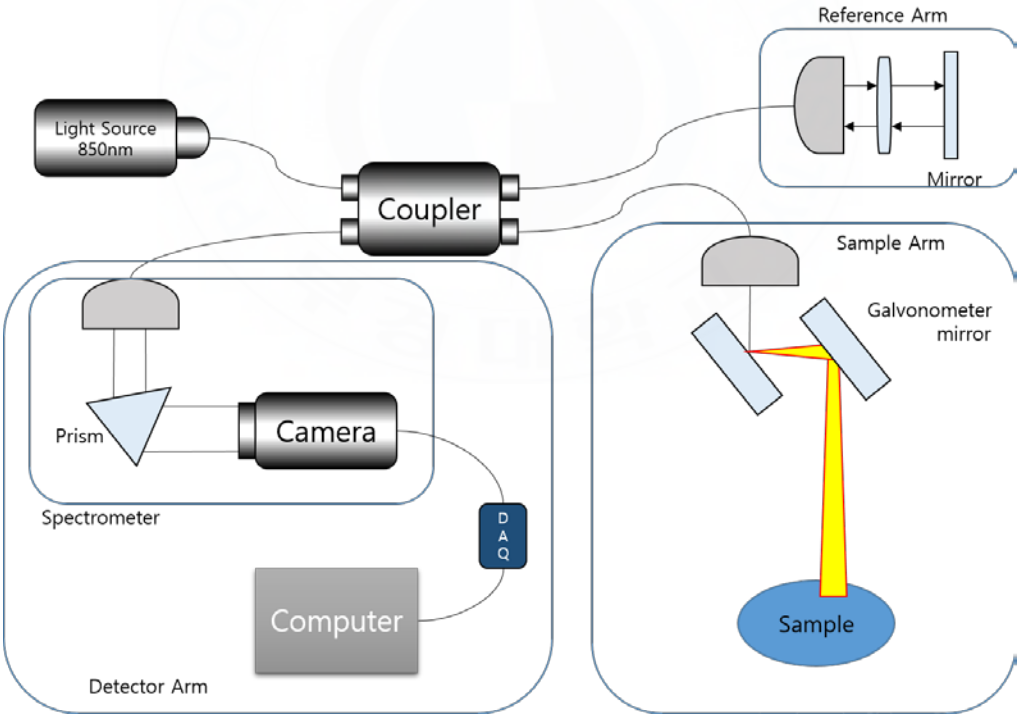

Figure II.1 The schematic of OCT. It based on Michelson interferometer. DAQ data acquisition.

Both arms had same Lens to reduce dispersion mismatch. The reflected lights at sample and the mirror went through coupler to

the detector arm. The light incident on the detector arm passed the collimator to make the light into parallel light at first. And then interference is made while the light passed through the Spectrometer. The light had a different diffraction angles for each wavelength, which was incident light on the line scan camera through the diffraction grating.

Optical coherence tomography of the mathematical principles were as follows. Coordinate system x, y, z can be expressed as shown in Figure Ⅱ.2 based on the end of sample arm. Y axis is defined as an incident light parallel to the depth direction, and the xz plane is defined as the plane perpendicular to the y−axis. A signal incident from the light source to the coupler was called the input signalU_{in}.

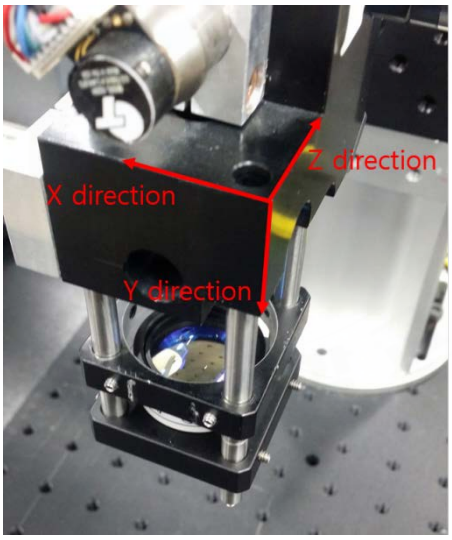

Figure II.2 In the coordinate system of the OCT sample arm.

s$(\omega)$was the amplitude of the light source, ω was frequency, θ was the phase accumulation within the interferometer.

$$U_{in}(\omega,t) = s(\omega)\exp[-i(\omega t-\theta)] \quad (1)$$

However, the system had considered only the relative phases of the two optical paths. Therefore, equation (1) could be expressed as equation (2) shows.

$$U_{in}(\omega, t) = s(\omega)\exp[-i(\omega t)] \quad (2)$$

The signal output from coupler was called U_{out}, signal to make for the reference arm was expressed U_r, signal to make for sample arm was defined U_s, that could be expressed as equation (3).

$$U_{out} = U_r + U_s \quad (3)$$

At this time, the frequency response function of the sample and each signal could be represented as in the following.

$$U_r(\omega, t) = \sqrt{\frac{1}{4}}U_{in}(\omega, t_r) = \sqrt{\frac{1}{4}}s(\omega)\exp(-i\omega t)\exp(i\frac{\omega}{c}2n_r l_r) \quad (4)$$

$$U_s(\omega, t) = \sqrt{\frac{1}{4}}\int_0^{\infty} a(y)U_{in}(\omega, t_s)dy \quad (5)$$

$$= \sqrt{\frac{1}{4}}s(\omega)\exp(-i\omega t)H(\omega, t)$$

$$\mathrm{H}(\omega, \mathrm{t}) = \int_0^{\infty} a(y)\exp\left[i\frac{\omega}{c}2n_s(l_s + y)\right]dy \quad (6)$$

n_r	A refractive index of reference arm
n_s	A refractive index of sample arm
c	The speed of light in air
l_r	The physical length from 2×2 coupler to a fixed mirror on the reference arm
$l_s + y$	The physical length from 2×2 coupler to a particle of tissue the sample arm
t_r	The sum of the time for the light to reach from light source to 2×2 coupler and the time for the light to shuttle between reference arm and 2×2 coupler.
t_s	The sum of the time for the light to reach from light source to 2×2 coupler and the time for the light to shuttle between sample arm and 2×2 coupler.
U_r	Signal of reference arm into 2×2 coupler

U_s	Signal of sample arm into 2×2 coupler
a(y)	Backscattering amplitude

Table II.1 The meaning of each symbol in the above equations (4), (5) and (6)

Equation (6) had represented a frequency response function of the sample arm. Because the light was reflected in the sample arm that had a different accumulated phase value. l_r physical length could be adjusted to satisfy $n_r l_r = n_s l_s$. It satisfies the equation meant to match the path length to the virtual image of a fixed mirror in the reference arm and the path length to the y−axis origin in the sample arm.

The light intensity was measured by the spectrometer, it could be expressed as a function of the frequency and time.

$$\mathrm{I(k,t)} = \frac{1}{\tau}\int_{-\frac{\tau}{2}}^{+\frac{\tau}{2}} U_{out}(k,t)U_{out}^{*}(k,t)dt \qquad (7)$$

$$= \frac{1}{4}S(k) + \frac{1}{2}S(k)\int_0^{\infty} a(y)\cos(2kn_s y)\,dy + \frac{1}{4}\int_0^{\infty}\int_0^{\infty} a(y)a\left(y^{'}\right)\exp[i2kn_s\left(y-y^{'}\right)dy\,dy^{'}$$

I	Light intensity
k	Wavenumber
y	A particle of tissue depth position in sample arm
y’	Another particle of tissue depth position in sample arm
τ	Exposure time of the spectrometer
S(k)	The spectral intensity of the light source
*	Conjugate complex number

Table II.2 The meaning of each symbol in the above equation (7)

The first term in equation (7) is meant the intensity of the reflected light from the reference arm. The light coefficient was fixed $\frac{1}{4}$ because perfect reflection mirror in reference arm and 2×2

coupler. The third term was the intensity of light reflected from the sample arm that was due to interference of reflected light from another location in the sample. Two above-mentioned terms of equation (7) were not considered because these were the light intensity of the reference arm and interference between the neighboring particles within a sample arm. However, the second term was a significant signal interference phenomenon of the reflected light from the sample and reference arms.

Increase in the y-axis depth was meant a high-frequency signal in the frequency domain. Quantity of pixels in the camera of spectrometer was finite according to the Nyquist sampling criterion. Therefore, it was difficult for the camera detects more than a predetermined high frequency. So it is necessary to minimize the length of the particles to the y-axis origin.

If the power spectral density of the light source according to the Gaussian distribution could be expressed as shown in equation (8).

$$\mathrm{S(k)} = P_0 \exp[-4 \ln 2 \frac{(k-k_0)^2}{\Delta k^2}] \tag{8}$$

k_0 is the center wavenumber, $\Delta \mathrm{k}$ is the width of the full width at half maximum(FWHM) in the wavenumber, P_0 is the maximum power at the center wavelength. Considering the second term in the equation (7) it could be expressed as follow.

$$\mathrm{I(k,t)} = \frac{1}{2} S(k) \int_0^{\infty} a(y) \cos(2kn_s y)\, dy \tag{9}$$

The first upper surface of the sample was set as the origin of the y-coordinate. Thus, if y is less than 0, it is $a(y) = 0$, which means the backscattering amplitude. Therefore, $\tilde{a}(y)$ has been introduced to the $a(y)$ to make an even function.

$$\tilde{a}(y) = \begin{cases} a(y) \\ a(-y) \end{cases} = \begin{cases} a(y) & if\ y \geq 0 \\ a(-y) & if\ y \leq 0 \end{cases} \tag{10}$$

In Equation (9) $a(y)$ was carried out a Fourier transform after substituted with $\tilde{a}(y)$. Equation (11) represents the Fourier transform domain from k to $2n_s y$.

$$F^{-1}[I(k,t)] = \frac{1}{4}F^{-1}[S(k)] + \frac{1}{8n_s}F^{-1}[S(k)] \otimes [\tilde{b}(\frac{\eta}{2n_s})] \qquad (11)$$

η is defined as $2n_s y$, and F^{-1} is the inverse Fourier transform, $\otimes$ means a convolution operator. 식 The second term of equation (11) represented a complex signal, and it meant a reflectance distribution according to the depth y. This could be obtained the structure of the sample image. In addition, the inverse Fourier transform of broadband bandwidth S(k) provides a narrow Gaussian distribution, and the FWHM is $8\ln\frac{2}{\Delta k}$ in the η area. The sensitivity of system and Signal Nosie Ratio (SNR) is calculated depth of sample using point spread function as in Figure 2.1.2. In addition, the system sensitivity roll-off was 5.747dB at 0.5mm depth, SNR is represented 103.8dB. Depth resolution is represented by the equation (12), according to the equation system has a depth resolution of 4um (in air).

$$\delta z = \frac{2\ln(2)}{\pi}\frac{\lambda_0^2}{\Delta\lambda} \qquad (12)$$

λ_0 is the center wavelength, $\Delta\lambda$ is the FWHM of the light source.

2 Sample arm

The sample arm was composed two-axis scanner, four system lens and objective lens in this study. Figure Ⅱ.3 was a two-axis scanner chamber and schematic diagram of four system lens in sample arm. The sample arm was composed of two Relay lens and two of the galvanometer mirrors and 45° tilted mirror, and the light was focused on the biological tissue through the objective lens.

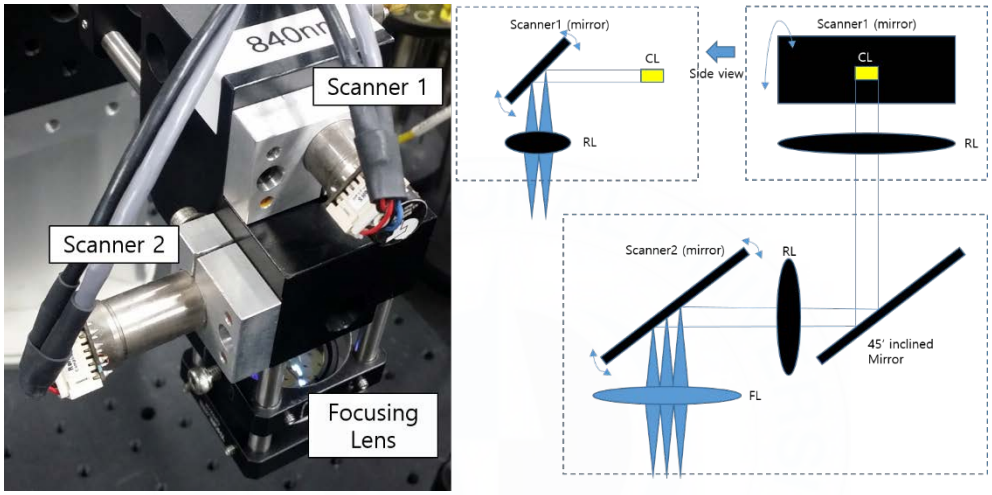

Figure II.3 The schematic diagram of sample arm. RL relay lens, CL collimator lens, FL focusing lens.

Figure Ⅱ.4 showed the numerical aperture (NA) of the objective lens, lateral resolution and depth of field. When the numerical aperture was increased, depth of field and focal size was decreased, but the lateral resolution was increased. Lateral resolution was shown in equation (13).

$$2\omega_0 = \frac{4\lambda}{\pi}\frac{f}{D} = \frac{2\lambda}{\pi}\frac{1}{NA} \qquad (13)$$

NA meant numerical aperture, f was the focal length of the objective lens, $2\omega_0$ was the beam spot size, the same word is the lateral resolution in the equation (13). This showed that the higher NA of the objective lens got better the lateral resolution. The low NA showed an increase of b to mean a depth of field in the equation (14).

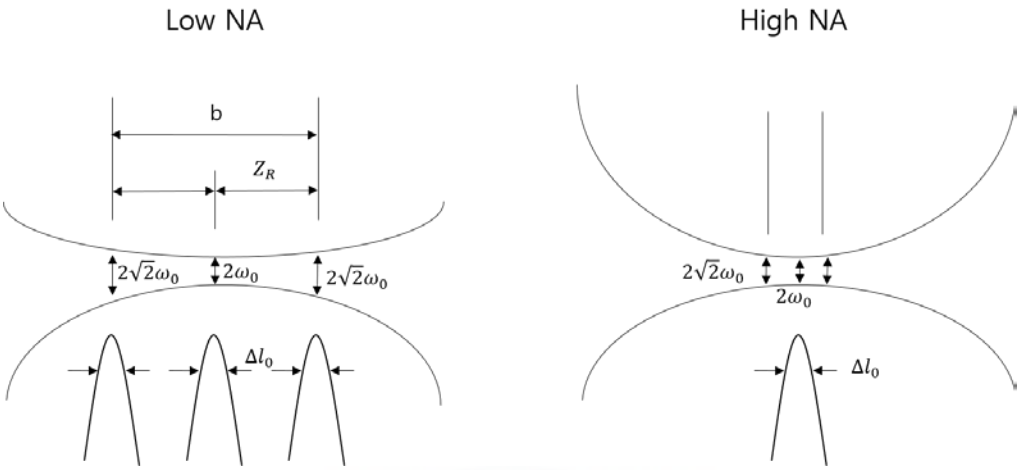

Figure II.4 Low numerical aperture (NA) shows longer depth of field than high NA. However, high NA has smaller beam spot size than low NA. Beam spot size associates with the traverse resolution.

$$\mathrm{b} = 2Z_R = \frac{\pi \Delta \omega_0^2}{\lambda} = \frac{14\lambda}{\pi}\frac{1}{NA^2} \qquad (14)$$

The incident light on the sample in this condition was the cause scattering or reflection by a different index of refraction within the sample. Some of the light scattered by the sample was lost, another light had entered into the spectrometer that was Incident on the numerical aperture of the focusing lens. It showed Figure Ⅱ.5 A-scan that the reflected light measured for making the graph from the sample after the light entered y-direction as depth direction at a point in the xz-plane of the sample. An A-scan is observed in the longitudinal direction at one point in the xz-plane of the sample equally above. It was defined as a B-scan, when the sample was scanned the x-axis using one of the galvanometer in the xz-plane as the Figure Ⅱ.5 B-scan. Z-axis was scanned using the other galvanometer mirror, then the three-dimensional image is created through amira software, it is defined as a C-scan. It is shown in Figure Ⅱ.5 C-scan.

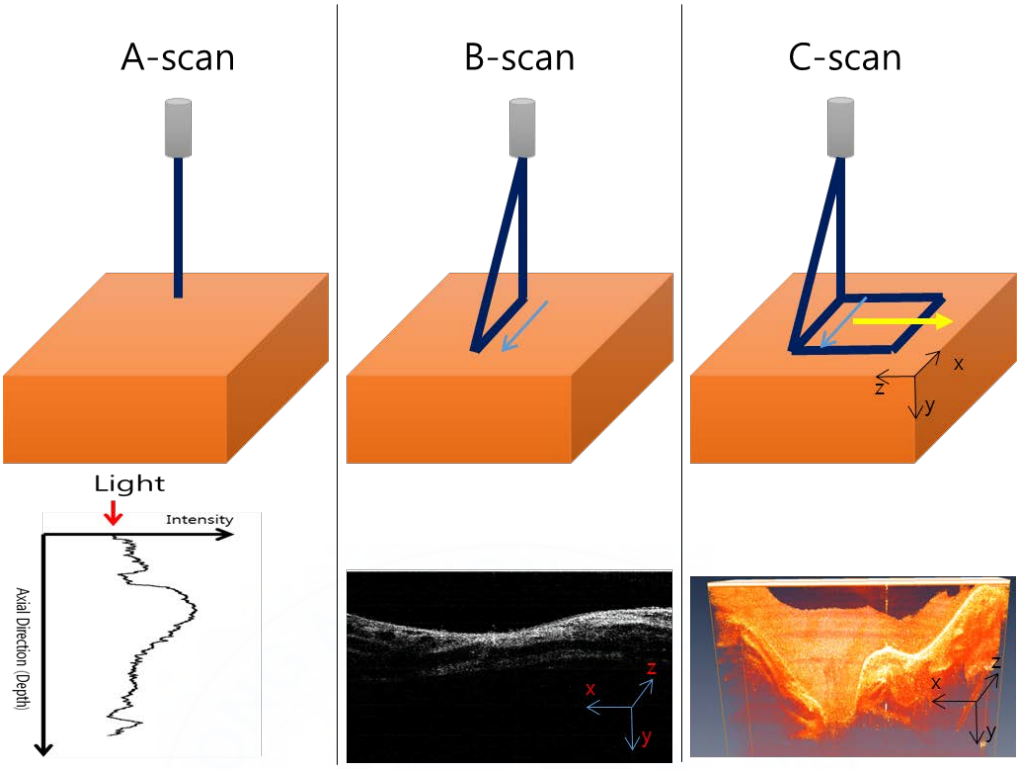

Figure II.5 OCT can obtain a two-dimensional or three-dimensional images. A-scan means to measure the depth direction from a point, and B-scan obtain a flat data while A-scan moving in one axis. Scanning once again the B-scan in a vertical axis, it is possible to acquire a three-dimensional image, which is called C-scan.

Figure Ⅱ.6 is a galvanometer mirror (Cambrige Technology Co., Ltd.) used in the study, Table 3 indicates the main characteristics. Galvanometer scanner driver is controlled by the analog input board (PCI-6711) and Visual C ++ Software.

Figure II.6 The galvanometer mirror, Model 6220H Optical Scanner

Rated Angular Excursion	40°
Rotor Inertia	0.125 gm*cm^2, +/− 10%
Thermal Resistance, Coil to Case	1℃/Watt, Max
Coil Resistance	2.79 Ohms, +/− 10%
Current, RMS	3.9A, Maximum
Current, Peak	20A, Maximum
Small Angle Step Response	200us, with appropriate CTI Y mirror
Linearity	99.9%, minimum, over 40° optical
Scale Drift	50PPM/℃, Maximum
Zero Drift	15 Microradians/℃, Maximum
Repeatability	8 Microradians, Maximum

Table II.3 Indicates the main characteristics of 6220H optical scanner

3 Reference arm

Reference arm was organized a collimator lens, an objective lens and mirror. That equipment make up same lenses with sample arm's because dispersion mismatch of minimum. Focal length of the focusing lens (achromatic doublet) by thorlabs Inc. is 35mm and the lens correct the chromatic aberration in reference arm. Focal length of the collimator lens by thorlabs Inc. is 11.07mm and numerical aperture (NA) of the lens is 0.26. Figure Ⅱ.7 is appeared reference arm. Objective lens and mirror set on removeable rails for easy to adjust about path difference to interference and all optic equipment was installed on the same axis for line up.

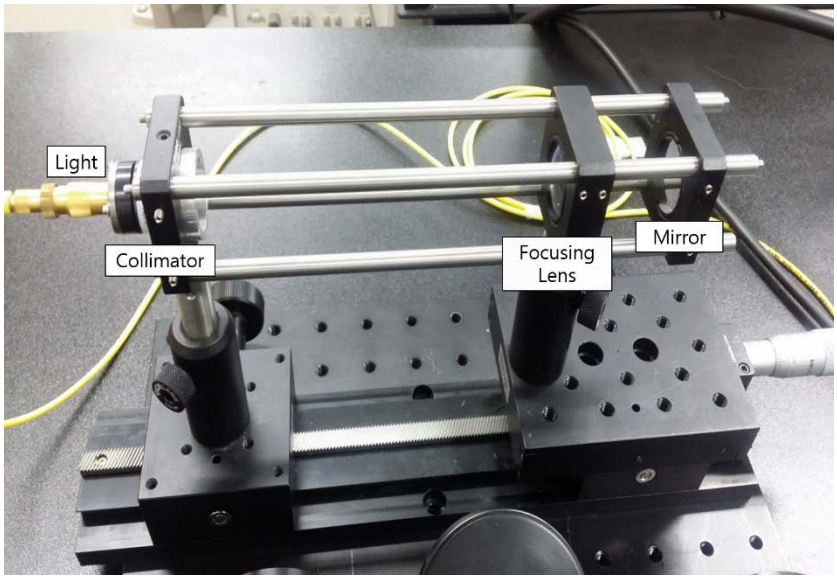

Figure II.7 Reference Arm.

4 Light source (Superluminescent LED)

The light source used in the experiment is broadband light sources based on a combination of two SLDs (Superluminescent LED, SLD) with slightly different center wavelengths. Center wavelengths of combined different lasers 840nm, and full width at half maximum (FWHM) is 120nm. Intensity and density of light wavelengths are shown in Figure Ⅱ.8.

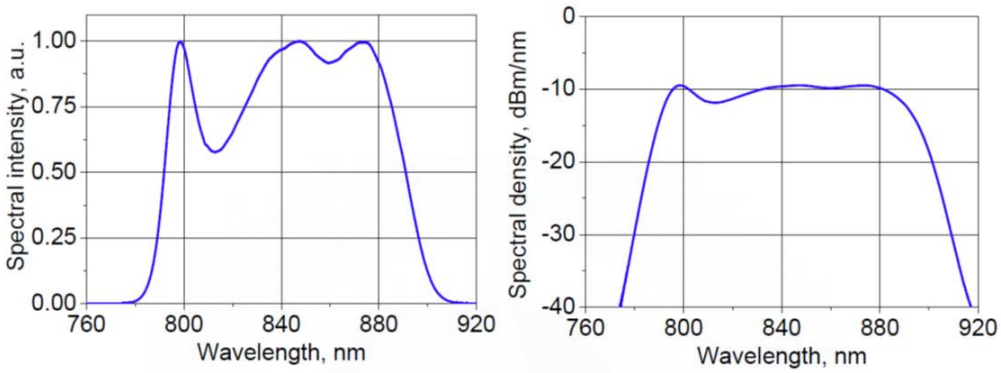

Figure II.8 Spectral intensity and density spectrum with wavelength at 10mW power level.

Coherence length of light source is 4.5 ㎛ and less in air. It means interference occurs in case optical path length gap of sample arm and reference arm within 4.5um.

Figure II.9 Light generator shape.

5 Spectrometer

5.1 Grating

The grating (Wasatch Photonics) is mounted on the spectrometer whose center wavelength is 840nm, grating diameter is 50.8mm, thickness is 6mm. Kind of transmission grating is a holographic type as 1800 l/mm.

$$\mathrm{a}(\sin\theta_i + \sin\theta_m) = m\lambda \qquad (15)$$

Equation (15) represents the grating equation, m is the order of diffraction through a grating, a is the gap between grids, θ_i is the incident angle, θ_m is the diffraction angle. Each parameter was applied θ_i to 49.1°, a to 1/1800mm, m to 1 in the experiment. (Figure Ⅱ.11)

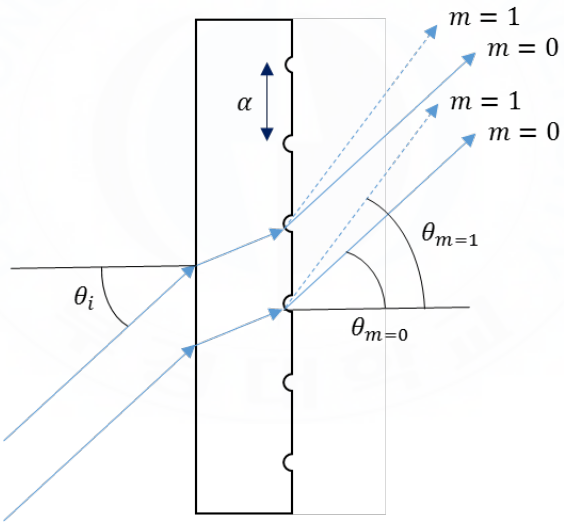

Figure II.10 Transmission grating concept diagram.

θ_m depends on the wavelength of light. Provided that knowing the wavelength of the incident, diffraction angle also can know. Figure Ⅱ.12 is the diffraction angle according to the wavelength of the used grating, is 49.1 ° at 840nm.

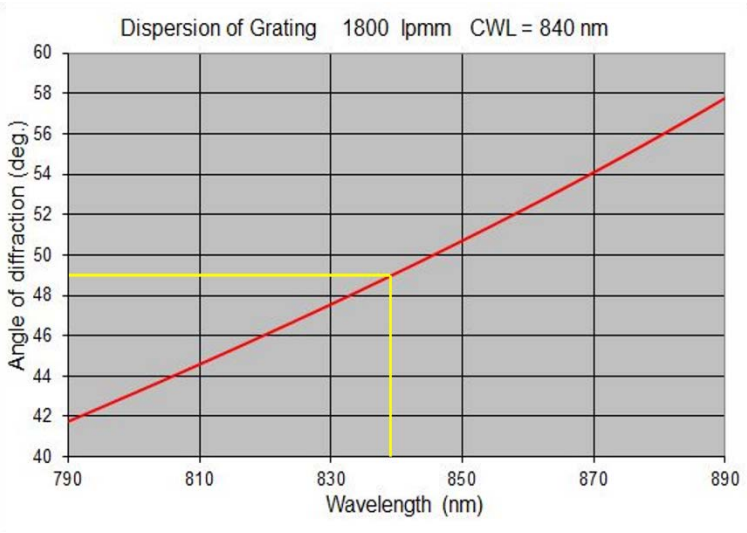

Figure II.11 Angle of diffraction on grating for 1800 line per mm.

Figure II.13 shows the diffraction efficiency according to the wavelength of a transmission grating. The diffraction efficiency is the highest when the center wavelength 840nm, decreases as far from the center wavelength.

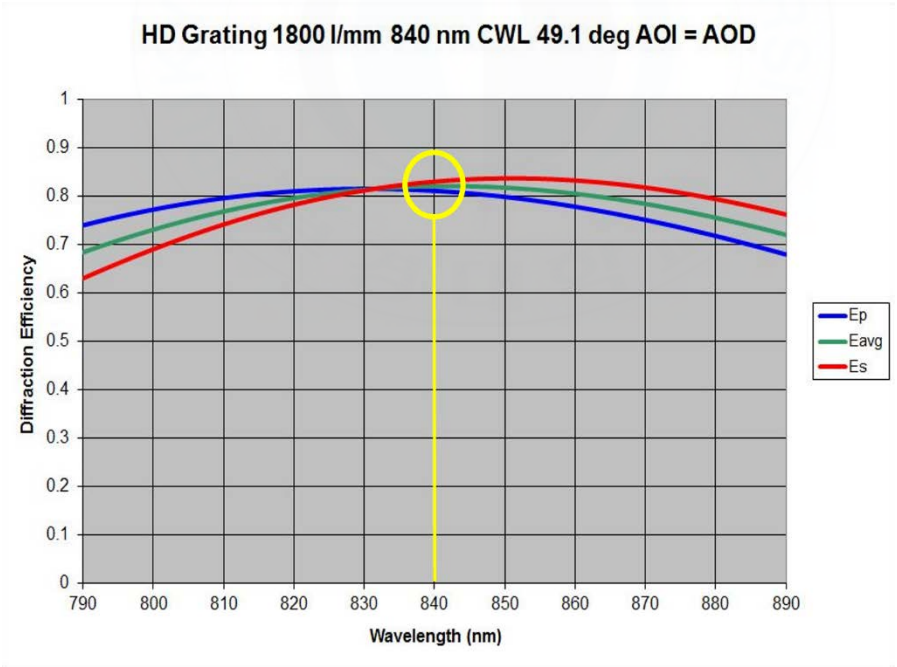

Figure II.12 Diffraction efficiency on grating for 1800 line per mm.

5.2 Line scan camera

The camera is a charge coupled device (CCD, spL4096, Basler Sprint) used in the study. Sensor of the camera is composed of two lines and each line is 4,096 pixels. The pixel size is 10um x 10um. The maximum line scan speed is 140kHz, the camera was set processing mode through the camera setup program (Camera Configuration Tool Plus, CCT +). Line processing mode is the vertical binning and the horizontal binning. Line processing mode was used as the vertical binning in this study.

Figure II.13 The structure of vertical binning for data process. (Source:spL4096-140km manual)

Figure Ⅱ.14 is a schematic diagram of a vertical binning, above all, the first pixel values of the line A is copied to the first pixel value of the line B. And then the signal of the two vertical pixels is processed as a single pixel. Therefore the pixel size of the vertical processing mode is a 10 um (H) x 20 um (V). The advantage of this mode, even if the amount of light that enters the camera can make image ever, and the reaction speed of the camera is fast because the processing of two lines as one line. In addition, syncronization mode of the camera is free run. Features of the free run mode are a method of processing information by the internal control signals without using an external trigger signal. The parameter which is determined by the control signal is a line period and the exposure time.

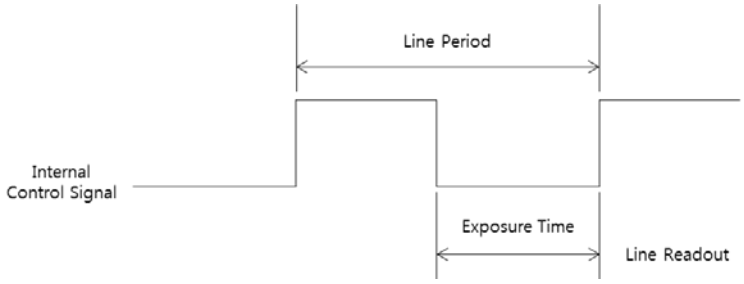

Figure II.14 Free run programmable mode. This operation is possible using the internal control signal. At a constant line period, the length of the signal reduces the exposure time was adjusted long, that increase was adjusted shorter the exposure time.

Figure Ⅱ.14 shows the process possible programming in free run mode. The square wave is generated inside the camera. The line period is defined from the first square wave generation point until the next time the square wave generation. And the exposure time is defined the interval between the end of the first square wave generation of next beginning square wave generation. Equation (16) is a line rate formula, it takes the inverse value of the line period.

$$\text{line rate} = \frac{1}{line\ period} \tag{16}$$

The line speed is 5.1um/s, and the exposure time is 2.7us in this study. Figure Ⅱ.15 shows the quantum efficiency over wavelengths. Pixels of the camera used in this experiment were made on a silicon substrate. Sensor made of the silicone material has a different energy transfer efficiency according to the wavelength of incoming light. Energy transfer efficiency is the highest when the wavelength 650nm, and the efficiency decreases with the wavelength. The efficiency of 37% at 840nm wavelength from the light source.

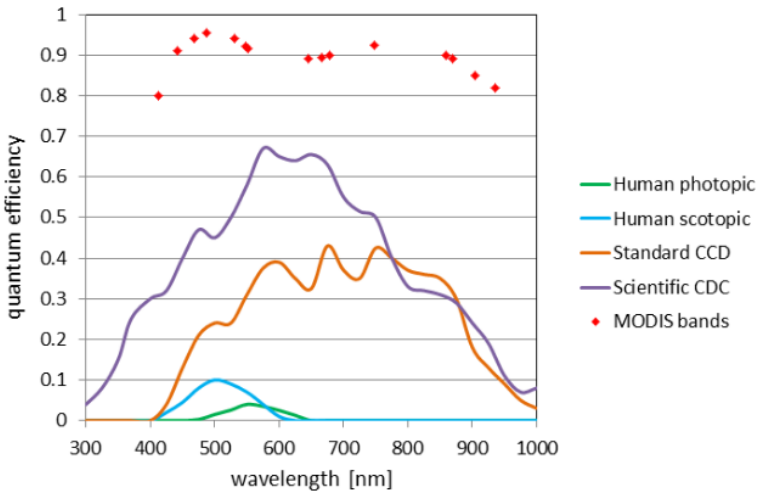

Figure II.15 Quantum efficiencies for various light detectors. The CCD has a quantum efficiency of 37% at 840nm wavelength. (Source: oceanopticsbook.info)

6 Computed tomography system

A computed tomography (CT) is a way to observe the entire image of a rabbit. CT scan was performed for the overall image recording of the lungs. It was taken using the product's Siemens SOMATOM Definition Flash which is installed in Kosin hospital. Product performance has slice thickness 0.6 mm as 128 slice scanner, was scanned using the B35f Mode. CT is shown in the following Figure Ⅱ.17.

Figure II.16 The CT model used in this study is a product of the SOMATOM Definition Flash made in Siemens. The B35f mode was used to apply a rabbit.

Increase the quality of the image in order to look at the reaction of asthma in the pulmonary local part, it must be capable of repeatedly conducted under the same conditions. The iso-pressure breath hold method was applied in order to limit the movement of breathing in vivo.

7 Summary of ventilator

This study uses Dual mode ventilator named TOPO of Kent Scientific Corporation. TOPO provides a variable setting of the respiration rate from 0 to 199.9 breaths per minute. It is allowed to adjust the inspiration % for inspiration of the total respiratory. The values mean inspiration-Expiration (I:E) ratio and range from 5 to 45% in increments of 5%. This can be changed by adjusting the respiratory waveform. The inspiration pressure is usually set in the range of 5-20cm of water pressure.

Figure II.17 Ventilator TOPO (Kent Scientific) for animals.

TOPO can output a signal for Pressure through a BNC connector. And the signal can be viewed through an oscilloscope as shown in the Figure Ⅱ.19.

Figure II.18 The ventilator can check the respiratory waveform with connecting an oscilloscope by BNC cable.

In order to perform a breath-hold, the respiratory rate was applied temporarily to zero. When performed using the Test lung, the oscilloscope can check the graph shown in the Figure Ⅱ.20.

Figure II.19 Oscilloscope waveform in breath-hold.

III. Methods

1 Subject preparation

The rabbits were used in the experiment New Zealand white rabbits and weight an average of them is about 3kg. Experimental animals were kept in individual cages where the temperature of 22 ± 2℃ and humidity of 55 ± 5 % maintained in the laboratory. The animals divided into experimental and control groups for experiment 3 weeks. Experimental groups were aspirated methacholine 5㎖ daily in 5㎎ / ㎖ concentration. The method of aspirated methacholine was the nebulizers using a humidifier (Ultrasonic Nebulizer, Omron). The control groups had to aspirate normal saline as the same way. Methacholine inhalation was conducted in the same method as in the following Figure Ⅲ.1.

Figure III.1 Rabbit preparation of inhaled methacholine.

2 Ventilator apply and computed tomography scan

The prepared rabbits were administered an appropriate amount (3mg/kg, IM) the anesthetic (zoletil 50) on the hip muscle for a CT scan. The rabbit's body was spread with anesthesia for ten minutes. It confirmed that anesthesia is normally composed, and performed endotracheal intubation in rabbits. This is made possible intubation tube of 3 or 4mm, determined to see the weight of the rabbit. The intubation tube is attached to a ventilator induces tidal normal breathing. The breathing pressure was maintained 16 ~ 17cmH2O, the respiration rate was maintained 20 times per minute.

The stable breathing in rabbit was led to inspiration breathing. The respiration rate was controlled to zero per minute after twice deep breathing (Pressure 28 ~ 29cmH2O), then a CT scan was conducted immediately. The breathing was returned to normal (pressure 16 ~ 17cmH2O) after a CT scan. The new breath-hold technique is practicable the only control respiration rate. Add simply than a conventional breath-hold method conducted breath-hold how the LabVIEW was applied to a ventilator breathing triggers.

Meanwhile, the CT scans conducted to B35f mode considering about small animals. Each refers to 3 resolutions of body kernel type, version number 5, fast scan mode.

GE mode	Siemens Mode	RMSD(mm^2)	PFD(mm^{-1})
Soft	B35f	0.01	0.00
Chest	B41f	0.01	0.01
Standard	B43f	0.01	0.00
Detail	B46f	0.04	−0.01
Bone, Edge	B75f	0.09~0.18	0.12~0.41
Lung	B80f	0.03	0.00

Table III.1 Siemens kernel to compare with GE kernel. (Source: resolveradiologic.com)

The following is a CT scan of the expiration breathing condition. The test lung enabled the expiration condition, lives as rabbits was difficult to make breath-hold because of functional residual capacity. But the ventilator made a similar expiration condition using inspiration condition

controlled pressure (5~8cmH2O), that could control breath-hold. The CT scan conducted same method of inspiration only controlled pressure. This is shown in the following Figure Ⅲ.2.

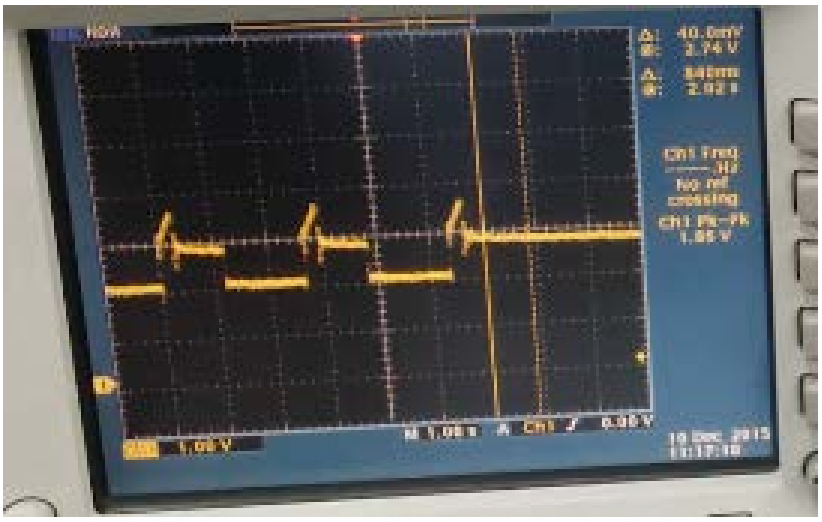

Figure III.2 Expiration condition, breath-hold waveform image.

3 Optical coherence tomography

One day rest gave the rabbit, prepared the OCT scanning. The method was same as the CT process that the intubation performed after anesthesia, and the rabbit's breath made stable applying a ventilator. OCT is difficult to pass the skin tissue for that reason made a window on lung as shown in Figure Ⅲ.3. Window refers to scrape until the remains, only a very thin layer of skin tissue and muscle tissue.

Figure III.3 The process of creating a window in the lungs of rabbits.

The breath-hold technique was same as the process of CT during OCT scanning. The scan was conducted in the OCT center wavelength is 845nm, axial resolution is 3.5um. Roll Off is a 106dB, Scanning speed has been conducted with 10 frames per second.

4 Biopsy after the sacrifice of the rabbits

The rabbit was sacrificed by injecting Zoletil on hip muscle within 30 minutes, after the OCT scanned. After to sacrifice, the lungs were extracted from the rabbit. The extracted lungs were scanned OCT to induce inspiration state pumping air into the lungs. (Figure Ⅲ.4) Finally, the lungs were sufficiently expanded then that put fixed in formalin solution. After which the lungs were requested pathologic examination for correlation analysis.

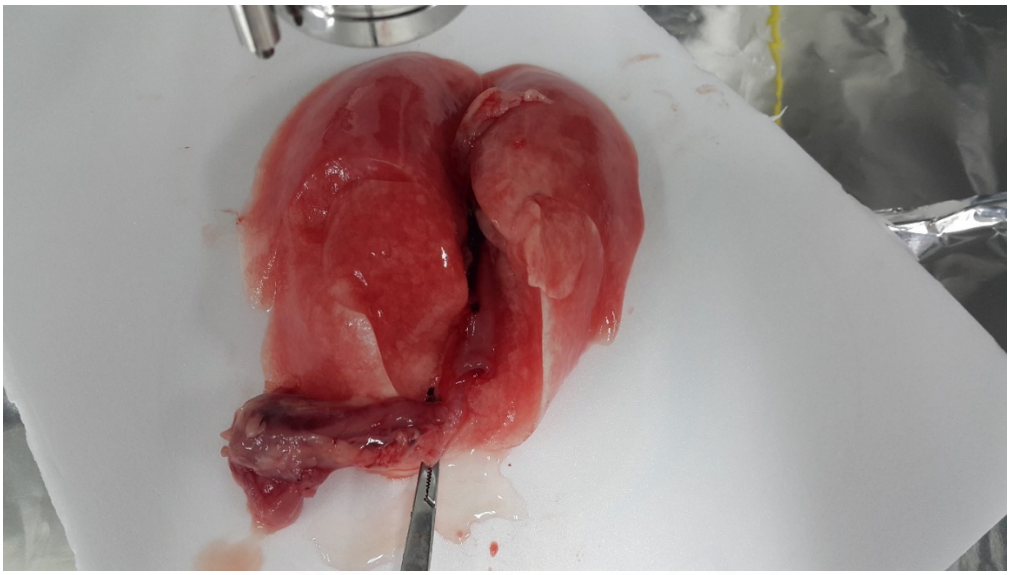

Figure III.4 The excised lungs of rabbits, while it is fixed after swelling to a CT scan.

IV. Result and Discussion

1 CT images analysis

These CT images are the experimental group and the control group about the aspiration methacholine shown in Figure Ⅳ.1. The control group has a uniform color of the whole lung. Part of the lungs image with high air ratio is displayed darker, because X-ray permeability was increased. The control group when the inspiration state alveoli shows similar color because of uniform expansion. On the other hand the experimental group shows a brighter image of the dorsal. The bright part of the image is guessed tissue or blood. This hypersensitivity reaction occurs with methacholine inhalation. It should respond to the alveoli to shrink or increase the amount of blood. A bright portion of the X-ray is considered above the reason.

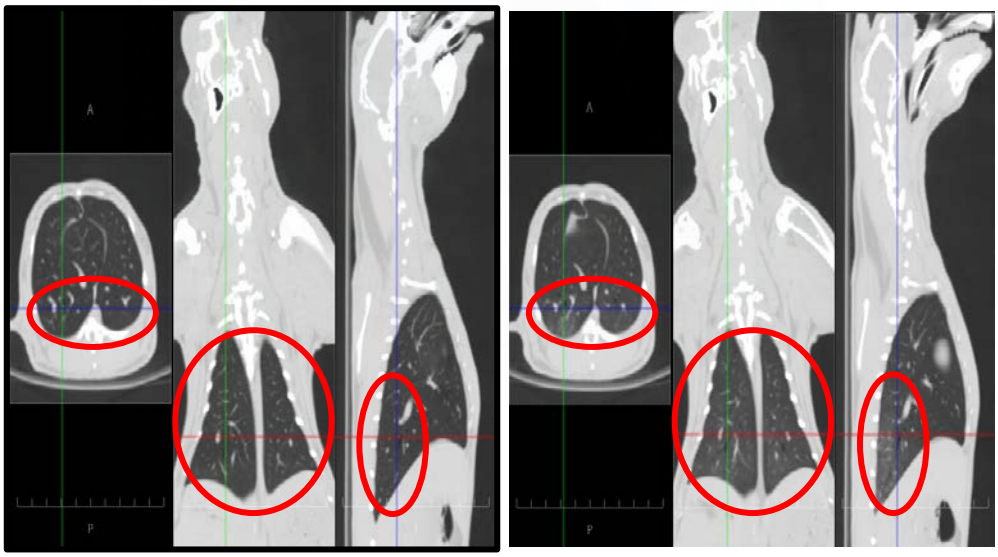

Figure IV.1 Control group CT images (left), Inhaled methacholine experimental group CT images (right).

The ventilator could be utilized to obtain the state of the inspiration animal images. In experiments with inhalation of methacholine were only dorsal part affected. The image of the pattern similar to the entire lung is expected to be found in diseases such as asthma.

2 OCT images analysis

The SD-OCT alveoli in vivo images show in Figure Ⅳ.2. Each figure is the upper contour of the surface of the lung, a curly black circle at the bottom of the image of the alveoli. The image of alveolar can be divided based on the inspiration and expiration. Also, it is divided into an experimental and control groups to methacholine inhalation, and thus the alveoli sizes differ. Conventional CT or MRI had been a big help find lesions watching the whole lung, meanwhile there were difficult to measure the size of the alveoli unit. However, OCT was able to distinguish each alveoli with high resolution.

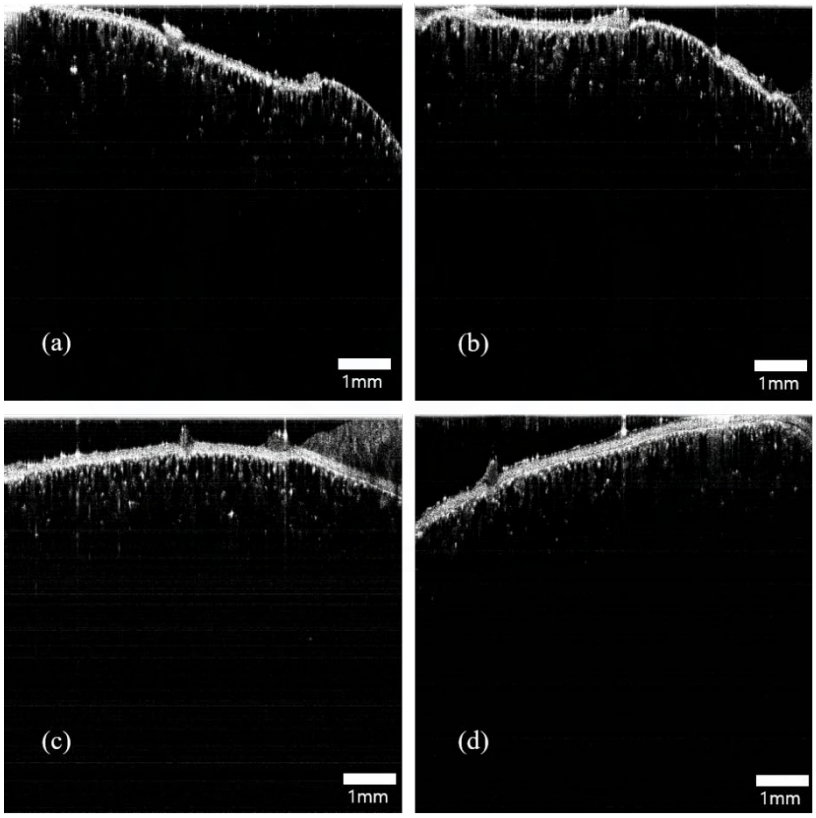

Figure IV.2 OCT image of the alveoli. The experimental of inspiration state (upper left), The experimental group expiration state (upper right), The control control of inspiration state (lower left), The control group of expiration state (lower right).

The excised lungs after the sacrifice the rabbits were taken the image in the injected air into the lungs. The SD-OCT scan was performed

under the same conditions as the previous scan with the experiment and control groups. Acquired images could be analyzed in the xz plane after reconstruction using the Amira three dimensions program such as Figure Ⅳ.3.

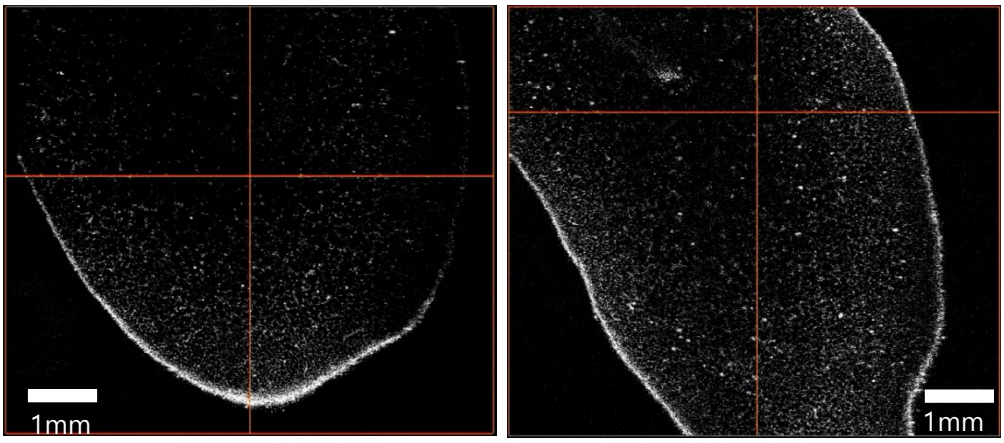

Figure IV.3 The image acquired by the xz plane after three-dimensionally re-constructed using Amira program an OCT image. The control group (left), the methacholine experimental group (right).

Using the Amira program could acquire an image of the desired location in depth direction y. The acquired image is confirmed very detailed image of the alveoli that are distributed among the distal lung. The control group showed left in the Figure Ⅳ.3 has regular alveoli size. However, the experimental group has irregular alveoli size, and alveolar size is small compared to the control group.

The alveolar size and volume of the lung between inspiratory and expiratory can be know certain difference by breath-hold technique developed through a ventilator. Image loss was generated by breathing in such conventional animal experiments. However, this experiment was to minimize image loss using the ventilator. It is also expected to increase the survival rate of the animal in experiments for a long time anesthesia.

3 Comparison histopathology and OCT images

The excised lungs and airways after OCT scanning were requested a pathology biopsy to determine the physiological changes.

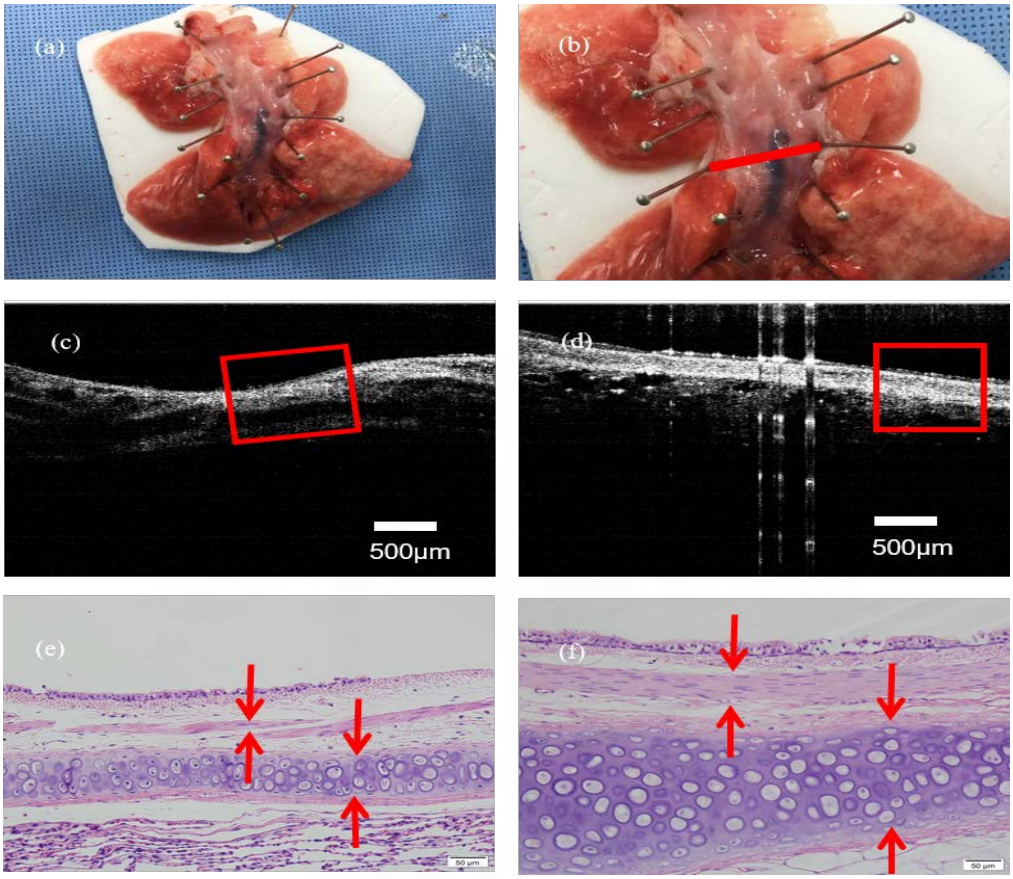

Figure IV.4 (A) Excised airway, (b) The target area (red line) right lower lobe (RLL), (c) The control group OCT image, (d) The experimental group OCT image, (e.) The control group pathology image, (f) The experiment group pathology image.

The image of lung edges of the experimental group (d) is bright compared to the control group (c) shown in the Figure Ⅳ.4. Brighter part of OCT image was scattered and reflected light more than darker part. In addition, the internal structure of the experimental group (f) inhaled methacholine is swelling compared with the control group (e) in pathologic analysis. This change makes data through accumulating which is expected to be a new way of diagnosis of asthma.

V. Conclusion

In this study, CT and OCT image studies were performed with breath-hold using a ventilator unlike a conventional approach, which induced airway constriction by methacholine inhalation for many people suffering from chronic diseases such as asthma in the world.

First, the experimental group rabbits that inhaled methacholine for 3 weeks with 5mg / ml concentration and the control group rabbit that inhaled normal saline same way applied the ventilator through endotracheal intubation after anesthesia. The ventilator led to inspiration and expiration state from normal state, and subject scanned using a CT at breath-hold. The control group was dark by and large, but the experimental group was bright at dorsal part. If the alveolar had contained air equally, X-ray image looked a steady dark. Because the alveoli shrank irregularly and the blood circulation increased from hypersensitivity reactions, accordingly the decline of X-ray transmission were displayed bright images.

Secondly, it was taken of the OCT in order to verify the alveolar image of the rabbit, which was prepared in the same way. A condition was created making window to the lungs of rabbits that could be taken an OCT image, and an experiment was conducted while adjusting the breathing ventilator. As with CT images, the alveoli of the control group were evenly distributed while the alveoli of the experimental group were atypically distributed and whose size also was not uniform, became uneven depending on the positions.

Third, air was injected into excised lungs after the rabbits sacrificed which were performed again OCT scan. Acquired image confirmed the image of the xz plane after three-dimensionally re-constructed using Amira software. The control group had a size of uniform alveoli, the experimental group had a size smaller non-uniform distribution of alveoli compared to the control group similar previous experiments.

Finally, it was compared analysis of the OCT image and pathological examination of the excised airway. The experimental groups overreacted to methacholine using pathological examination, it could be confirmed that the swelled tissue cells compared to the control group. The tissue of the experimental group appeared brighter, it was found that the swollen tissue by pathological examination was more scatter and reflect light.

Through a series of experiments, we confirmed the possibility of research methods by OCT or CT image in asthma. If an image acquisition method developed into harmless direction in the human body and non-invasive, the method was expected to be able to present a new direction for the asthma diagnostic method.

VI. Acknowledgement

2011년도에 학부를 졸업 하고, 가정형편으로 대학병원에 취업하여 의공기사로 업무를 수행하다가 못 다한 꿈을 위하여 2014년도에 처음으로 대학원에 입학하여, 하나의 마침표를 찍게 되었습니다. 많은 분들의 염려와 걱려 속에서 무사히 하나의 과정을 마치게 된 것에 감사를 드리며, 그 동안 표현 하지 못하고, 마음 속으로만 생각했던 감사의 표현을 이 짧은 글을 통해서나마 전하고 싶습니다.

먼저 제가 학부생일 때부터 많은 가르침을 주신 김정구 교수님께 감사의 말을 드립니다. 교수님의 고분자실험실에서 대학원이 어떤 곳인지 알게 되었고, 여러 가지 고민이 많았던 저에게 대학원의 길을 알려주셨습니다. 제가 대학원을 시작하게 된 가장 큰 영향을 주신 것 같습니다. 그리고 해운대백병원 시설부의 조한복 이사님, 정진상 부장님, 김종선 과장님, 정원일 대리님, 홍덕기 주임님 모두에게 감사 드립니다. 항상 바쁘고, 정신 없는 시설부였는데, 일과 시간 이후에 대학원을 갈 수 있게 배려해주시고, 옆에서 항상 응원 해주셨기 때문에 제가 끝까지 포기 없이 올 수 있었던 것 같습니다. 그리고 안예찬 교수님께 감사 드립니다. 아무런 준비 없이 시작하게 된 대학원 생활이었는데, 처음 저를 면담 해주신 인연으로 지도교수님이 되어주시고, 다른 대학원생들에 비해 부족한 저를 위해 많은 편의를 봐주시고, 학업에서도 열정적인 가르침에 큰 감명을 받았습니다. 그 모습을 앞으로 제 롤 모델로 삼아 더 정진하도록 하겠습니다. 강현욱 교수님과 정원교 교수님에게도 감사의 마음을 전합니다. 남들보다 늦은 시작으로 많이 부족한 저에게 어떻게 보면 과분할 정도로 많은 기회를 주시고, 존중해주시고, 항상 안부를 먼저 물어봐 주시는 모습은 제게 귀감이 되었습니다. 고신대학교의 옥철호 교수님, 김성원 교수님, 이해영 교수님에게 모두 감사 드립니다. 실험의 작은 부분부터 임상적용에 대한 해박한 지식으로 친절하게 알려주시고, 실험에 참여하기에 아직 많이 부족한 저를 항상 챙겨주셔서 너무 감사합니다. 또한 학부생 시절부터 항상 옆에 있어준 동아리 친구들, 이제는 서른이 넘어 형, 동생이라기 보다는 친구 같은 버팀목이 되어주는 사람들, 저의 결혼식을 위해서 먼 곳에서까지 와준 친구들, 앞으로도 우리의 우정이 영원히 반짝이길 바랍니다. 가족이라는 이름의 어머니와 아버지, 형 어릴 때부터 욕심쟁이였던 제가 하고 싶어 했던 일을 묵묵

히 지켜 봐주시고, 지지해주셔서 너무 감사합니다. 지금도 한 가정의 가장이 되었지만 부모님의 눈에는 철부지 애기 같을 겁니다. 그래도 실망시키진 않을 테니 걱정 마시고, 앞으로도 든든한 지원군이 되어주시길 바랍니다. 마지막으로 나의 평생의 동반자 혜정이, 저를 믿어주고, 배려해줘서 너무 고맙습니다. 2014년과 지금은 상황이 많이 달라졌지만 옆에서 항상 같은 자리에서 믿음을 주는 사람이 있기 때문에 저도 이런 결정을 할 수 있었고, 앞으로도 나아 갈 수 있는 힘이 됩니다. 앞으로도 부족하지만 제 곁에서 항상 응원해주길 바라며, 저도 우리 가정의 행복을 위해 최선을 다하겠습니다. 사랑합니다.

지금까지 저에게 영감을 주고, 여러 가지 면에서 도움을 주신 많은 분들을 일일이 거명하지 못하여 아쉽지만 마음속으로는 항상 고마운 마음을 간직하고 있습니다. 앞으로도 최선을 다해서 목표한 바를 이루는 것이 고마움을 보답하는 길이라고 생각하며 제 위치에서 최선을 다하도록 하겠습니다.

2016. 7

김이근

VII. Reference

Ahn, Kangmo, Jihyun Kim, Ho Jang Kwon, Yoomi Chae, Myung Il Hahm, Kee Jae Lee, Yong Mean Park, So Yeon Lee, Manyong Han, and Woo Kyung Kim. 2011. "The Prevalence of Symptoms of Asthma, Allergic Rhinoconjunctivitis, and Eczema in Korean Children: Nationwide Cross-Sectional Survey Using Complex Sampling Design." *Journal of the Korean Medical Association* 54 (7): 769–78. doi:10.5124/jkma.2011.54.7.769.

Akbari, O, R H DeKruyff, and D T Umetsu. 2001. "Pulmonary Dendritic Cells Producing IL-10 Mediate Tolerance Induced by Respiratory Exposure to Antigen." *Nature Immunology* 2 (8): 725–31. doi:10.1038/90667.

Aysola, Ravi, Eduard E. De Lange, Mario Castro, and Talissa A. Altes. 2010. "Demonstration of the Heterogeneous Distribution of Asthma in the Lungs Using CT and Hyperpolarized Helium-3 MRI." *Journal of Magnetic Resonance Imaging*. doi:10.1002/jmri.22388.

Beasley, Richard, U. Keil, E. Von Mutius, and N. Pearce. 1998. "Worldwide Variation in Prevalence of Symptoms of Asthma, Allergic Rhinoconjunctivitis, and Atopic Eczema: ISAAC." *Lancet* 351 (9111): 1225–32. doi:10.1016/S0140-6736(97)07302-9.

Chinn, S R, E a Swanson, and J G Fujimoto. 1997. "Optical Coherence Tomography Using a Frequency-Tunable Optical Source." *Optics Letters* 22 (5): 340–42. doi:10.1364/OL.22.000340.

Coxson, Harvey O., Brendan Quiney, Don D. Sin, Li Xing, Annette M. McWilliams, John R. Mayo, and Stephen Lam. 2008. "Airway Wall Thickness Assessed Using Computed Tomography and Optical Coherence Tomography." *American Journal of Respiratory and Critical Care Medicine* 177 (11): 1201–6. doi:10.1164/rccm.200712-1776OC.

de Boer, Johannes F, Barry Cense, B Hyle Park, Mark C Pierce, Guillermo J Tearney, and Brett E Bouma. 2003. "Improved Signal-to-Noise Ratio in Spectral-Domain Compared with Time-Domain Optical Coherence Tomography." *Optics Letters* 28 (21): 2067–69. doi:10.1364/OL.28.002067.

Etzel, Ruth A. 2003. "How Environmental Exposures Influence the Development and Exacerbation of Asthma." *Pediatrics* 112

(1): 233–39. doi:10.1542/peds.112.1.S1.233.

Fercher, A F, W Drexler, C K Hitzenberger, and T Lasser. 2003. “Optical Coherence Tomography – Principles and Applications.” *Reports on Progress in Physics* 66 (2): 239–303. doi:10.1088/0034-4885/66/2/204.

Fujimoto, J G, M E Brezinski, G J Tearney, S A Boppart, B Bouma, M R Hee, J F Southern, and E A Swanson. 1995. “Optical Biopsy and Imaging Using Optical Coherence Tomography.” *Nat Med* 1 (9): 970–72. doi:10.1038/nm0995-970.

GAMBICHLER, T, G MOUSSA, M SAND, D SAND, P ALTMEYER, and K HOFFMANN. 2005. “Applications of Optical Coherence Tomography in Dermatology.” *Journal of Dermatological Science* 40 (2): 85–94. doi:10.1016/j.jdermsci.2005.07.006.

Golubovic, B., B. E. Bouma, G. J. Tearney, and J. G. Fujimoto. 1997. “Optical Frequency-Domain Reflectometry Using Rapid Wavelength Tuning of a Cr4+:forsterite Laser.” *Optics Letters* 22 (22): 1704–6. doi:10.1364/OL.22.001704.

Gupta, Sumit, Salman Siddiqui, Pranab Haldar, James J Entwisle, Dean Mawby, Andrew J Wardlaw, Peter Bradding, Ian D Pavord, Ruth H Green, and Christopher E Brightling. 2010. “Quantitative Analysis of High-Resolution Computed Tomography Scans in Severe Asthma Subphenotypes.” *Thorax* 65 (9): 775–81. doi:10.1136/thx.2010.136374.

Huang, D, EA A Swanson, CP P Lin, J. S Schuman, W. G Stinson, W Chang, M. R Hee, et al. 1991. “Optical Coherence Tomography.” *Science* 254 (5035): 1178–81. doi:10.1126/science.1957169.

Jung, Woonggyu, Daniel T McCormick, Yeh-Chan Ahn, Ali Sepehr, Matt Brenner, Brian Wong, Norman C Tien, and Zhongping Chen. 2007. “In Vivo Three-Dimensional Spectral Domain Endoscopic Optical Coherence Tomography Using a Microelectromechanical System Mirror.” *Optics Letters* 32 (22): 3239–41. doi:10.1364/OL.32.003239.

Lam, Stephen, Anthony M D Lee, Pierre Lane, Keishi Ohtani, Calum MacAulay, Nina Varfolomeva, Linda Hui, Harvey O Coxson, and J Mark Fitzgerald. 2013. “Optical Coherence Tomography Imaging Of Asthmatic Airways Before And After Thermoplasty.” In *A110. LATE BREAKING ABSTRACTS IN OBSTRUCTIVE*

LUNG DISEASES, A6014–A6014. American Thoracic Society International Conference Abstracts. American Thoracic Society. doi:doi:10.1164/ajrccm-conference.2013.187.1_MeetingAbstracts.A6014.

Leitgeb, R, C Hitzenberger, and Adolf Fercher. 2003. "Performance of Fourier Domain vs Time Domain Optical Coherence Tomography." *Optics Express* 11 (8): 889. doi:10.1364/OE.11.000889.

Miller, Rachel L., and Shuk Mei Ho. 2008. "Environmental Epigenetics and Asthma: Current Concepts and Call for Studies." *American Journal of Respiratory and Critical Care Medicine*. doi:10.1164/rccm.200710-1511PP.

Moffatt, M F, I G Gut, F Demenais, D P Strachan, E Bouzigon, S Heath, E von Mutius, et al. 2010. "A Large-Scale, Consortium-Based Genomewide Association Study of Asthma." *The New England Journal of Medicine* 363 (13): 1211–21. doi:10.1056/NEJMoa0906312.

Pitris, C, M E Brezinski, B E Bouma, G J Tearney, J F Southern, and J G Fujimoto. 1998. "High Resolution Imaging of the Upper Respiratory Tract with Optical Coherence Tomography: A Feasibility Study." *American Journal of Respiratory & Critical Care Medicine* 157 (5 Pt 1): 1640–44.

Puliafito, Carmen A., Michael R. Hee, Charles P. Lin, Elias Reichel, Joel S. Schuman, Jay S. Duker, Joseph A. Izatt, Eric A. Swanson, and James G. Fujimoto. 1995. "Imaging of Macular Diseases with Optical Coherence Tomography." *Ophthalmology* 102 (2): 217–29. doi:10.1016/S0161-6420(95)31032-9.

Schmitt, Joseph. 1999. "Optical Coherence Tomography (OCT): A Review." *IEEE Journal of Selected Topics in Quantum Electronics* 5 (4): 1205–15. doi:10.1109/2944.796348.

Steen, N, A Hutchinson, E McColl, M P Eccles, J Hewison, K A Meadows, S M Blades, and P Fowler. 1994. "Development of a Symptom Based Outcome Measure for Asthma 109." *BMJ* 309 (0959-8138 (Print)): 1065–68.

Tearney, G J, M E Brezinski, B E Bouma, S a Boppart, C Pitris, J F Southern, and J G Fujimoto. 1997. "In Vivo Endoscopic Optical Biopsy with Optical Coherence Tomography." *Science (New York, N.Y.)* 276 (5321): 2037–39. doi:10.1126/science.276.5321.2037.

Tearney, Guillermo J, Mark E Brezinski, Brett E Bouma, Stephen A Boppart, Costas Pitris, James F Southern, and James G Fujimoto. 1997. “In Vivo Endoscopic Optical Biopsy with Optical Coherence Tomography.” *Science* 276 (5321): 2037–39. doi:10.1126/science.276.5321.2037.

Thomas, Abraham C., Erin N. Potts, Ben T. Chen, Deborah M. Slipetz, W. Michael Foster, and Bastiaan Driehuys. 2009. “A Robust Protocol for Regional Evaluation of Methacholine Challenge in Mouse Models of Allergic Asthma Using Hyperpolarized 3He MRI.” *NMR in Biomedicine* 22 (5): 502–15. doi:10.1002/nbm.1362.

Welzel, J., E. Lankenau, R. Birngruber, and R. Engelhardt. 1997. “Optical Coherence Tomography of the Human Skin.” *Journal of the American Academy of Dermatology* 37 (6): 958–63. doi:10.1016/S0190-9622(97)70072-0.

Williamson, Jonathan P., Robert A. McLaughlin, William J. Noffsinger, Alan L. James, Vanessa A. Baker, Andrea Curatolo, Julian J. Armstrong, et al. 2011. “Elastic Properties of the Central Airways in Obstructive Lung Diseases Measured Using Anatomical Optical Coherence Tomography.” *American Journal of Respiratory and Critical Care Medicine* 183 (5): 612–19. doi:10.1164/rccm.201002-0178OC.

Wills-Karp, M, J Santeliz, and C L Karp. 2001. “The Germless Theory of Allergic Disease: Revisiting the Hygiene Hypothesis.” *Nature Reviews. Immunology* 1 (1): 69–75. doi:10.1038/35095579.

Zhang, Jian, Peter D Paré, and Andrew J Sandford. 2008. “Recent Advances in Asthma Genetics.” *Respiratory Research* 9 (1): 4. doi:10.1186/1465-9921-9-4.

A preclinical study on airway remodeling under methacholine provocation using OCT and CT with breath-hold techniques

Yikeun Kim

Department of Biomedical Engineering, The Graduate School,
Pukyong National University

Abstract

Many asthma studies have been conducted analyzing the computed tomography (CT) images. However, the pathogenesis of asthma has not been clearly revealed yet. This study proposes a new methodology to study the ventilator-simulated inhaling and exhaling pulmonary images in vivo after breath-holding the study subject.

The imaging technologies used in this study are CT and Optical Coherence Tomography (OCT). CT analyzes the multiple layers of X-ray images. And the new technology OCT has proven its harmlessness to the human body and the high resolution of the image. The study intended to use these methods to examine the images of the lung and the alveoli in the breath-hold state. The ventilator-simulated breath-hold technique enabled the collection and analysis images reduced noise of respiration in animal studies.

The examiner induced methacholine to remodel the subject rabbit's airway. After the anesthesia the normal breath was simulated at its maximum pressure of 17cmH2O; the inspiration was done at its maximum pressure of 28 cmH2O; the breath-hold was simulated by controlling the respiration rate from 15 to 0; then return to the normal breath. The same simulation cycle was used for the expiration breath-hold at its maximum pressure of 7cmH2O. During the two breath-holds the CT and OCT images were taken and significant result was observed on the lung and alveoli.